Journal of Molecular Graphics and Modelling 44 (2013) 253–265

Contents lists available at ScienceDirect

Journal of Molecular Graphics and Modelling

journal homepage: www.elsevier.com/locate/JMGM

Crystal structure, stability and spectroscopic properties of methane and CO_2 hydrates

Ruben Martos-Villa[a], Misaela Francisco-Márquez[b], M. Pilar Mata[c], C. Ignacio Sainz-Díaz[d,*]

[a] Facultad de Ciencias del Mar y Ambientales, Universidad de Cádiz, Av. República Saharaui s/n, 11510 Puerto Real, Spain
[b] UPIICSA, Instituto Politécnico Nacional, Col. Granjas México, 08400 México D. F., Mexico
[c] Instituto Geológico y Minero de España, La Calera 1, 28760, Tres Cantos, Madrid, Spain
[d] Instituto Andaluz de Ciencias de la Tierra, CSIC-Universidad de Granada, Av. de las Palmeras, 4, 18100 Armilla, Granada, Spain

ARTICLE INFO

Article history:
Received 20 February 2013
Received in revised form 11 June 2013
Accepted 26 June 2013
Available online 5 July 2013

Keywords:
Methane hydrate
Clathrates
CO_2 hydrates
Molecular-dynamics

ABSTRACT

Methane hydrates are highly present in sea-floors and in other planets and their moons. Hence, these compounds are of great interest for environment, global climate change, energy resources, and Cosmochemistry. The knowledge of stability and physical–chemical properties of methane hydrate crystal structure is important for evaluating some new green becoming technologies such as, strategies to produce natural gas from marine methane hydrates and simultaneously store CO_2 as hydrates. However, some aspects related with their stability, spectroscopic and other chemical-physical properties of both hydrates are not well understood yet. The structure and stability of crystal structure of methane and CO_2 hydrates have been investigated by means of calculations with empirical interatomic potentials and quantum-mechanical methods based on Hartree–Fock and Density Functional Theory (DFT) approximations. Molecular Dynamic simulations have been also performed exploring different configurations reproducing the experimental crystallographic properties. Spectroscopic properties have also been studied. Frequency shifts of the main vibration modes were observed upon the formation of these hydrates, confirming that vibration stretching peaks of C–H at 2915 cm^{-1} and 2905 cm^{-1} are due to methane in small and large cages, respectively. Similar effect is observed in the CO_2 clathrates. The guest–host binding energy in these clathrates calculated with different methods are compared and discussed in terms of adequacy of empirical potentials and DFT methods for describing the interactions between gas guest and the host water cage, proving an exothermic nature of methane and CO_2 hydrates formation process.

1. Introduction

Gas hydrates are crystalline compounds consisting of gas molecules encaged in cavities of a hydrogen-bonded network of water molecules. Gas hydrates are characterized by the general formula $X{\cdot}nH_2O$, where X is the guest molecule within a water cage, and n is the hydration number per guest molecule. Depending on the properties of the guest gas molecules and the conditions of the hydrate formation procedure, three different gas hydrate structures can be obtained: sI, sII and sH [1]. The cubic sI structure consists of 46 water molecules per unit cell, forming two dodecahedron (5^{12}) and six tetradecahedron ($5^{12}6^2$) cages (Fig. 1) and is formed when small guest molecules (having a molecular diameter of 4.2–6 Å) are trapped, such as methane, ethane, carbon dioxide, and hydrogen sulfide.

Methane is a hydrophobic molecule and its solubility in water is rather low and methane molecules tend to aggregate when they are solvated in water. However, in special conditions water/methane system can form clathrates increasing this solubility more than thousand times. Medium pressures, low temperatures and high methane gas concentration in water are needed to form methane hydrates [2]. These conditions can be reached in permafrost regions and sediments of the ocean floor in outer continental margin regions [3]. The current estimation of carbon contained in worldwide methane accumulations has given different values [4]. Based on a mechanistic model, Buffet and Archer [5] yielded 3×10^{18} g, which is double the energy contained in the total fossil fuel reserves.

Hydrocarbon trapped on marine sediments, methane hydrate and gases plays an important role in the terrestrial system. The possibility of a large scale hydrate destabilization and the release of methane into atmosphere (being a powerful greenhouse gas) would cause a great impact on Earth's climate, and would dramatically increase the temperature of the planet [6]. Carbon isotopic data from the geologic record suggests that vast methane releases

* Corresponding author. Fax: +34 958552620.
E-mail address: ignacio.sainz@iact.ugr-csic.es (C.I. Sainz-Díaz).

1093-3263/$ – see front matter © 2013 Elsevier Inc. All rights reserved.
http://dx.doi.org/10.1016/j.jmgm.2013.06.006

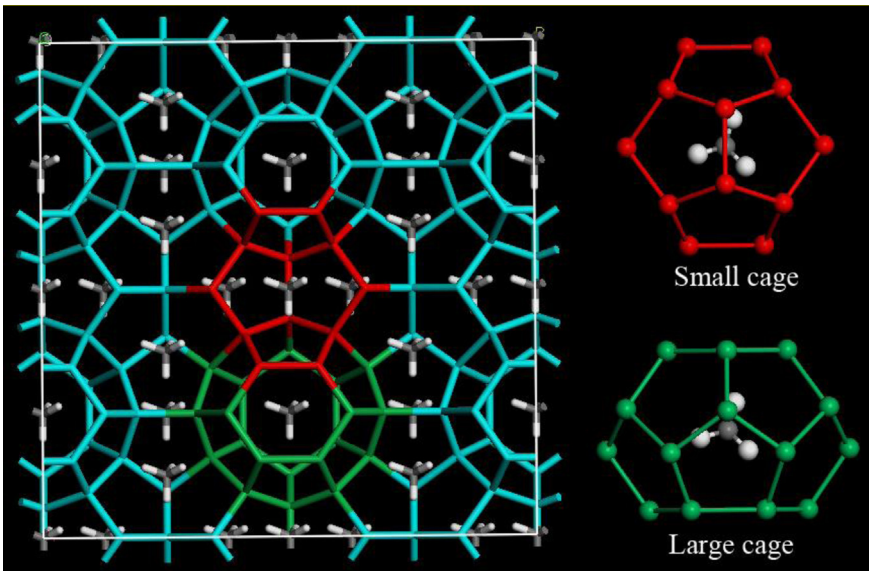

Fig. 1. Schematic framework of cages extracted from the crystal lattice of methane hydrates. Red balls represent O atoms from water molecules. H atoms of water molecules are not represented for a better understanding.

in the past were related to abrupt past-climate changes [7]. Catastrophic future scenarios have been recently proposed if the arctic methane hydrates are released to the atmosphere [8]. Reserves of methane gas forming hydrates are such that if only a 10% of them were released, they would cause an impact equivalent to multiply by 10 the actual amount of atmospheric CO_2 [9]. On the other hand, these natural gas hydrates are considered as a potential major energy resource, although the high dispersion and complexity of those deposits make necessary to overcome technical challenges to enable an economical extraction of natural gases [10]. Hence, the knowledge of stability and physical–chemical properties of methane hydrate crystal structure is important for evaluating some new green becoming technologies such as, strategies to produce natural gas from marine methane hydrates and simultaneously store CO_2 as hydrates.

In the solar system, methane hydrate is considered to be one of the major constituents of outer planets and their moons, such as Neptune, Uranus and Titan [11]. Also, the recent detection of methane at an average 15 ppb level in the Martian atmosphere from Mars Express and Earth-based observations [12] suggests that methane currently is being produced. An interesting possibility is that methane is released to the atmosphere from decomposition of subsurface clathrate layers [13].

A better understanding of the molecular mechanism leading to hydrate crystallization and decomposition is a crucial part of the practical problems mentioned above. Experimental studies of methane hydrates are not easy owing to the working handicaps in conditions of stability of these compounds, and it is difficult to obtain sufficient reliable data. On the other hand, theoretical studies of computational mineralogy can be very useful to understand and interpret experimental results.

Molecular calculations on the structural and thermodynamic properties of gas hydrates have been performed using quantum mechanics methods [14–16] with cluster models [17,18] and crystal lattice models trying to describe the weak guest–host interactions in the hydrates [19,20] Classical Molecular Dynamics techniques have been used with different force fields to calculate the crystal structure [21,22], and to describe different properties of methane hydrates like mechanisms of nucleation [23,24] and crystal growth kinetics [25,26]; mechanisms of decomposition [27,28]; and vibration spectroscopy [29–31].

Vibrational spectroscopy is a useful tool for determining many aspects of guest–host relationships. Most of experimental Raman studies on methane hydrates [32–34] assigned two peaks of $\sim$2905 cm^{-1} and $\sim$2915 cm^{-1} to the symmetric C–H stretching mode of methane in large and small cage respectively [35–37]. This assignment was based only on peak intensities but seems to be contradictory because methane molecule on large cage has more transitional freedom of motion, like methane gas whose peak appears at $\sim$2917 cm^{-1} [38], than methane in small cage. The opposite has been reported in methane hydrate [39] and in methane trapped in silica cages [40]. Conflicting with the assignments done on experimental works described above, computer simulations carried out by Greathouse et al. [29] found that vibrational behaviour of methane molecules occupying large cages are similar to that of methane gas. Those computational results are in agreement with other experimental studies carried out by Seitz et al. [41] and Hester et al. [42].

The aim of this work is to contribute to a better understanding of the crystalline structure of methane and CO_2 hydrates and the guest–host interactions in the clathrate comparing different theoretical approaches.

1.1. Models and computational methodology

Quantum chemical calculations of molecules were performed using Hartree–Fock (HF) approximation and second-order Moeller–Plesset approximation at the all electron (MP2). The molecular electronic structure was calculated with a split-valence triple-ζ basis set augmented with polarization functions for all atoms including H atoms (HF/6-311G** and MP2/6-311G** levels) as implemented in the Gaussian03 program package [43]. All geometries were fully optimized using the Berny analytical gradient method. No geometry constraint was applied on the molecules. Normal mode analyses were carried out at the same level to confirm the nature of the various stationary points, finding only positive eigenvalues for minima. Zero point correction was applied in all energy calculations of molecules and cluster models.

Ab initio total energy calculations of the periodic crystal model were performed using Density Functional Theory (DFT) methods based on plane-waves by means of the CASTEP code [44] and the numerical atomic orbital (NAO) methodology implemented

in the SIESTA program [45]. We used the generalized gradient approximation (GGA) with the Perdew–Burke–Ernzerhof (PBE) parameterization of the exchange-correlation functional [46] and the local density approximation (LDA) with CA–PZ (Ceperley and Alder–Perdew and Zunger) parameterization [47,48]. In some calculations with SIESTA a revised PBE functional (RPBE) [46] was also used. Core electrons were replaced by norm-conserving pseudopotentials [49] in the SIESTA calculations and by ultrasoft pseudopotentials in the CASTEP calculations. Pseudopotentials simulate the interaction between valence electrons and cores (nuclei plus core electrons) and neither core electrons nor core wave functions have to be included explicitly. With this approximation the valence wave functions are substituted by pseudo-wave functions that do not present strong oscillations in the core region. Calculations were restricted to the Γ point in the irreducible wedge of the Brillouin zone. In all structures, all atoms were relaxed by means of conjugated gradient minimizations at constant volume. In SIESTA, the basis sets are made of strictly localized numerical atomic orbitals (NAOs) with a localization cut-off radii corresponding to an energy shift of 270 meV. These basis sets used in this work are double-Z polarized (DZP) following the perturbative polarization scheme. For the H and O atoms, we used basis-sets and pseudopotentials both optimized by Fernández-Serra and Artacho [50]. The vibration frequencies of gas hydrate clusters and the crystal lattice calculated with SIESTA were obtained with VIBRA by analysis of forces generated by finite atomic displacements. This approach was successfully validated in previous calculations on phyllosilicates [51].

A uniform mesh with certain plane-wave cut-off energy is used to represent the electron density, the local part of the pseudopotential and the Hartree and exchange-correlation potentials. Preliminary calculations have been performed for SIESTA and CASTEP in order to tune the best calculation conditions including this cut-off energy. Total energy calculations were performed with different cut-off energy values (from 100 Ry to 600 Ry in steps of 50 Ry for SIESTA, and from 250 eV to 700 eV in steps of 50 eV for CASTEP) in the Γ point. In both cases, the energy decreases with the increase of the cut-off energy reaching asymptotically to a constant value. Hence the decrease of total energy is practically negligible for cut-off energy values higher than 500 Ry in SIESTA and 350 eV in CASTEP. The same behavior was found with 2 and 3 k-points of the Brillouin zone. Therefore, we performed optimizations in the Γ point with cut-off energy of 150 Ry in SIESTA and 350 eV in CASTEP and the total energy of the optimized structures was performed with 2 k-points and cut-off energies of 550 Ry in SIESTA and 350 eV in CASTEP. These conditions are consistent with our previous work [52] and have a higher computational level than previous calculations with SIESTA on methane hydrates [53].

For the study of the diffusion of one methane molecule in the cages of the clathrate crystal lattice and the transition state (TS) of this diffusion from small cage to large one, DFT calculations were performed using DMol^3 code [54] based on atomic orbitals, within the Material Studio package [55], with the local electronic density approximation (LDA), double ζ numerical basis sets plus polarization functions on all atoms and pseudopotentials with core-corrections. These calculations were performed at the Γ point of the Brillouin zone of the crystal. All atomic positions were fully optimized at constant volume. The search of TS was performed employing a combination of LST/QST algorithms [56] with subsequent conjugate gradient methods.

Since the above quantum mechanical methods can have difficulties to describe the dispersive interactions and weak adsorption interactions, empirical interatomic potentials have also been used for comparison, in order to determine the energy landscape. These empirical potentials were used within a Force Field (FF) that has recently been optimized by Heinz et al. [57] based on CVFF (consistent valence force field) and we named it CVFFH. These FF yielded good results in phyllosilicates with organics [58]. The atomic charges were taken from charges calculated at ab initio MP2/6-311G** level and associated to the electrostatic field (ESP) with the method of Merz and Kollman [59] for free molecules. Preliminary studies of methane hydrate with these atomic charges (−0.492 and +0.123 e^- for O and H respectively) were compared with atomic charges taken from Greathouse et al. [29] (−0.4 and +0.1 e^- for O and H respectively) and empirical charges calculated with the Qeq method [60] based on the equilibration of atomic electrostatic potentials with respect to an empirical local charge equilibration (−0.587 and +0.146 e^- for O and H respectively). Although there are no major changes between the three sets of atomic charges, the structure of hydrate optimized with ESP charges has crystal lattice parameters and geometry closer to experimental.

Different calculation conditions were tuned with respect to the 12-6 (CVFF) Lennard-Jones potentials and with the van der Waals and Coulomb interactions. We found that the van der Waals atom based interactions with a cut-off of 15.5 Å and the Ewald summation for Coulomb interactions yielded the best results and we used these conditions in this work. For these CVFFH calculations, we employed the Discover program within the Material Studio package [55].

A periodic model of the crystal structure of methane hydrate was generated based on experimental atomic coordinates and lattice cell parameters [61]. The cluster models of methane hydrate were generated extracting each hydrate cage with methane from the crystal lattice (Fig. 1). The initial cluster models and crystal lattice model of CO_2 clathrate was generated using the methane clathrate models substituting the methane molecules by CO_2.

The calculations of methane and CO_2 molecules in SIESTA, CASTEP and with CVFFH were performed including the molecule in a periodical box with the same cell parameters as in the adsorption scenario (11.95 Å in a cubic cell) that is large enough for avoiding intermolecular interactions between vicinal cells.

In all cases the adsorption energy has been calculated in the usual way: $U_{\text{adsorption}} = U_{\text{molecule in hydrate cage}} - (U_{\text{empty hydrate cage}} + U_{\text{molecule}})$, where U is the internal energy of the each system fully optimized at constant volume.

2. Results and discussion

2.1. Gas hydrate clathrate as a cluster

The main component of these clathrates is the water structure. Many theoretical models have been developed in order to describe water geometry and behavior. However, no water model available is able to reproduce all the water properties with good accuracy yet. In this work, preliminary calculations with empirical Force Fields were performed with the SPC model [62] included in CVFFH Force Field. This model assumes a point charge located in each atom of water molecule [63] and it applies charges of +0.41 and −0.82 e^- for hydrogen and oxygen respectively. Molecular Dynamics simulations of a disordered system composed of 100 water molecules (300 atoms), in NPT conditions at 298 K and 0.1 MPa with steps of 1 fs during 20 ps were performed. The simulation results were analyzed by means of Radial Distribution Functions (RDF) of O–O, O–H, and H–H pairs taken from 400 configurations sampled each 50 fs of the simulations and comparing them with experimental results obtained by neutron diffraction in the same conditions by Soper [64] (Fig. 2). The O–O RDF shows that the average distance between closest oxygen atoms is 2.7 Å matching the experimental data. The H–H RDF shows average distance between hydrogen atoms at 2.4 and 3.8 Å reproducing the experimental data. The O–H RDF shows two main peaks at 1.7–1.8 Å and 3.2–3.3 Å corresponding to hydrogen bonds between neighboring water molecules being

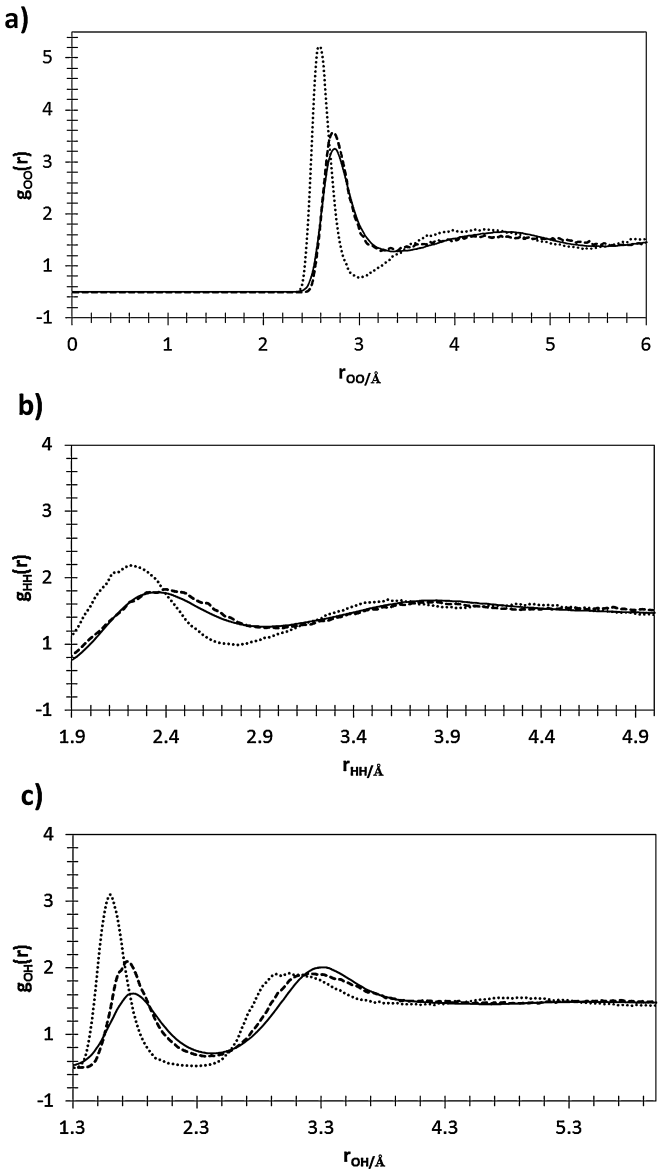

Fig. 2. Comparison of the RDF profiles of O–O (a), O–H (b), and H–H (c) atoms in the calculated water block model. Solid line corresponds to experimental data [64], dashed line corresponds to calculated values with the SPC model, and the dot line is the calculated with the TIP4P model.

the first peak more intense and narrow than the experimental one. Average density based on the results of Molecular Dynamics simulations of this block of water is 1.025 g cm^{-3} according with density of liquid water under similar conditions. For comparison purposes, we performed the same calculations using the TIP4P water model finding an average density for this bulk of water of 1.17 g cm^{-3} that is slightly larger than that obtained with SPC and the experimental one. In Fig. 2, the RDF profiles of the structure optimized with the TIP4P model are included, observing that small differences are found with respect to the experimental one. Therefore, the methodology used in these calculations with the SPC model can be considered valid to reproduce aqueous media for our system.

In order to evaluate the viability of the different calculation methods used, the molecular structure of methane at gas phase was analyzed after optimizations at HF/6-311G** and MP2/6-311G** levels with GAUSSIAN03, GGA/PBE/DZP level with SIESTA, GGA/PBE and LDA/CA-PZ levels with CASTEP, and CVFFH methods (Table 1). All methods reproduce the experimental values of HCH angle and H–C bond length; although HF yields a shorter CH bond length; and SIESTA and LDA yield a longer CH bond than the experimental one.

A cluster model composed of one 5^{12} cage of the methane hydrate crystal was generated with one methane molecule surrounded by 20 hydrogen-bonded water molecules extracting a cage from the experimental crystal structure, thus reducing the number of atoms and, therefore, the computational cost (Fig. 1) and the above calculation methods were applied. Similar cluster model was used previously with ab initio calculations [14]. Another cluster model for the large cage, $5^{12}6^2$, was generated also from the crystal lattice (Fig. 1). However, its optimization could converge only at HF/6-311G** level.

Table 1 shows the main geometrical features of the cluster model of the 5^{12} cage optimized by different calculation methods comparing with experimental data [61]. Results obtained with all methods are in agreement with experimental values, but small differences can be noted. Water molecule is better reproduced by CVFFH and DFT than HF, where the O-H bond length is too short and the hydrogen bonds are slightly shorter than experimental one. On the contrary, LDA calculations yields too long O–H bond and shorter H bonding than experimental value. Non-bonding distances between methane and water molecules are very well reproduced with CVFFH, being shorter those obtained by LDA approximation and with SIESTA (GGA/PBE) calculations.

In Table 1, the values of the large cage model optimized at HF level was included for comparison with those of the small cage model optimized at the same HF level. The hydrogen bonds between the water molecules in the large cage, $5^{12}6^2$, are longer than in the small cage. This is related with that the O–H bonds are shorter in the large cage than in the small cage. The non-bonding C...O and H_m...O distances are longer in the large cage than in small cage due to the larger size of the $5^{12}6^2$ cage. The C–H_m bond length is slightly longer in the large cage than in small one.

Similar geometrical features were found for the CO_2 hydrate cluster models with d(C–O) bond length values (1.136 Å, 1.180 Å, 1.225 Å by HF/6-311G**, GGA/PBE and CVFFH calculations, respectively) close to experimental one (1.166–1.180 Å) [65]. In the small cage model the CO_2 molecule remains in the center of the cage like in the methane one. However, in the large cage, the CO_2 molecule can have different possible positions out of the center, whereas the methane molecule in the $5^{12}6^2$ cage remains close to the center of the cage. This is consistent with high disorder of the CO_2 molecule in the hydrate clathrate lattice found experimentally [66].

2.2. Gas hydrate crystal structure

The use of cluster models is very interesting to compare properties of confined molecules. However, they have some limitations due to the boundary edges effect. In the above clusters, all water molecules are coordinated with other 3 water molecules, while in the crystal they are coordinated to four water molecules. Then, a unit cell of methane hydrate crystal (structure SI) [61] was generated including 178 atoms, 46 water and 8 methane molecules (Fig. 1) and all atoms positions were optimized at constant and variable volume, applying different simulation methods: based on DFT (CASTEP and SIESTA), and based on empirical interatomic potentials (CVFFH). In CVFFH calculations, the SPC model for water molecules was applied.

Firstly in order to evaluate the different theoretical methods used, we optimized the methane hydrate crystal structure at constant experimental volume comparing with experimental data [61] by using RDF of the main atomic pairs. In this case, RDF profiles were calculated for Hw–Hw (distances between hydrogen atoms of water molecules); O–O (distances between oxygen atoms), Hw–O (distance between hydrogen and oxygen of water molecules), and C–O (distance between C atoms of methane and O atoms of water

Table 1
Main geometrical features (average values for bond lengths and average values of the shortest non-bonding distances; distances in Å and angles in°) of methane hydrate cluster (small cage, 5^{12}) after full optimization with different computational methods. Values of methane gas are in brackets (H_w and H_m are H atoms of water and methane molecules, respectively).

Features	Exp[a]	HF[b]	GGA/PBE[c]	PW/GGA[d]	PW/LDA[d]	CVFFH[e]
d(H_w–O)	1.015	0.955, 0.948[f]	1.000	1.010	1.060	1.031
d(H_w...O)	1.772	1.952, 2.050[f]	1.710	1.657	1.535	1.709
d(C–H_m)	1.070, 1.098[g] (1.091)	1.083, 1.084[f] (1.084, 1.091[h])	1.083 (1.101)	1.086 (1.089)	1.099 (1.096)	1.089 (1.090)
d(C...O)	3.860, 3.950[i]	4.011, 4.100[f]	3.855	3.846	3.534	4.006
d(H_m...O)	2.922	2.867, 3.095[f]	2.789	2.811	2.467	2.985
H–C–H	109.5 (109.5)	109.5, 109.7[f] (109.5)	109.5 (109.5)	109.5 (109.5)	109.5 (109.5)	109.5 (109.5)

[a] From experimental crystal structure obtained from X-ray diffraction [61].
[b] Calculated with HF/6-311G**.
[c] Calculated with SIESTA.
[d] Plane waves methods using CASTEP.
[e] Calculated with CVFFH force field.
[f] Cluster model of large $5^{12}6^2$ cage.
[g] Experimental data from Tse [53].
[h] Based on MP2/6-311G** calculations.
[i] From Du et al. [14].

molecules) (Fig. 3). Experimental RDF profiles were calculated from the experimental crystalline structure [61]. The calculated structures reproduce the experimental RDF profiles. The main differences are observed in the C–O RDF profile due to the possible disorder of the methane molecules in the cages. The peak centered at 4 Å corresponds to the methane in small cages and it is more intense and narrow than that centered at 4.5 Å corresponding to large cages. This is due to the smaller space and higher constraints for movement of methane molecule in the small cage than in the large cage. This can be observed clearly in the experimental model where the disorder degree is lower. In the models calculated with CVFFH and SIESTA the peak at 4.5 Å is very broad indicating a high degree of disorder of methane molecule in large cages. In models calculated with plane-waves, the disorder of methane is so high than it is not possible to distinguish the C–O peak of the small cages and large cages. Nevertheless, the peak values of all calculated crystal structures are according to those of experimental one [67].

The main geometric features of the atoms in the hydrate crystal lattice calculated with different methods are compared with those which we extracted from experimental crystal lattice. These calculated values are closer to experimental ones than in the cluster model (Table 2) as it was expected. The plane-wave methods show a too large C–H bond length of methane molecules. The C...O and H_m...O distances are larger in large cages than in small cages as it was expected. In general the H_m...H_w distances are within a wider range than in H_m...O, however considering the shortest distances for each case the H_m...H_w distances are shorter than the H_m...O ones. This is remarkable and indicates that we have to consider the H_m...H_w and H_m...O interaction forces when we evaluate the interactions between methane and water molecules (see later). In all calculation methods, the C–H_m bond length is slightly longer in the large cages than in small cages. This fact is interesting because it is not easy to know experimentally this bond length due to the high disorder degree of the methane molecules in the large cage. In fact there are two experimental values reported being different, 1.070 Å (extracted from the crystal structure resolved from X-ray and neutron diffraction) [61], and 1.098 Å [53] without distinguishing the small and large cages and our result can explain some spectroscopic properties as we will discuss later.

In a second step, we optimized the clathrate crystal structures at variable volume in order to explore the reliability of the different methods used. The X-Ray Diffraction (XRD) patterns were calculated and compared with experimental XRD, obtaining similar characteristics, reflection positions and relative intensities in all cases, corroborating that crystalline structure of methane hydrate can be successfully reproduced using these methods. Lattice parameters of calculated methane hydrate unit cell have also been compared (Table 3). It can be observed that the closest values to experimental [61,68] are obtained with SIESTA, whereas the LDA approximation tends to make lattice parameters shorter than experimental. In the SIESTA results, the RPBE functional yields values closer to experiment than the PBE ones. These values are

Table 2
Main geometrical features (distances in Å) of methane hydrate crystal lattice after full optimization at constant volume (experimental cell parameters) with different computational methods (H_w and H_m are H atoms of water and methane molecules, respectively). Average values for bond lengths and average values of the shortest non-bonding distances, values in brackets correspond to maximum peak values within distance intervals.

		Exp[a]	CVFFH[b]	GGA/PBE[c]	PW/GGA[d]	PW/LDA[e]
d(H_w–O)		1.015	1.025	0.995	0.995	1.020
d(H_w...O)		1.772	1.765	1.770	1.775	1.785
d(C–H_m)	Small cage	1.070	1.089	1.072	1.088	1.095
	Large cage	1.070, 1.098[f]	1.090	1.085	1.090	1.098
d(H_m...H_w)	Small cage	2.570–3.355 (2.685)	2.605–3.320 (2.730)	2.450–3.045 (2.485)	2.535–3.250 (2.840)	2.495–3.450 (2.870)
	Large cage	2.700–5.250 (3.750)	2.760–5.120 (3.780)	2.615–4.950 (3.725)	2.730–5.730 (3.375)	2.545–5.650 (3.405)
d(C...O)	Small cage	3.745–4.235 (3.995), 3.950[g]	3.675–4.300 (3.885)	3.425–4.088 (3.715)	3.665–4.255 (3.885)	3.635–4.100 (3.825)
	Large cage	4.235–4.625 (4.505)	4.300–4.755 (4.485)	4.100–4.935 (4.545)	4.315–4.765 (4.465)	4.105–4.885 (4.345)
d(H_m...O)	Small cage	2.700–3.085 (2.945)	2.905–3.445 (3.095)	2.615–3.205 (2.885)	2.805–3.285 (3.045)	2.645–3.245 (3.055)
	Large cage	3.155–3.900 (3.300)	3.485–4.085 (3.675)	3.305–3.905 (3.675)	3.325–4.095 (3.875)	3.265–3.885 (3.665)

[a] Extracted from experimental crystal structure [61].
[b] Calculated with CVFFH force field.
[c] Optimized using SIESTA.
[d] Calculated with plane-waves using CASTEP and GGA with $E_{cut\text{-}off}$ = 350 eV.
[e] Calculated with plane-waves with CASTEP and LDA, $E_{cut\text{-}off}$ = 700 eV.
[f] Experimental data from Tse [53].
[g] From Du et al. [14] without distinguishing the cage types.

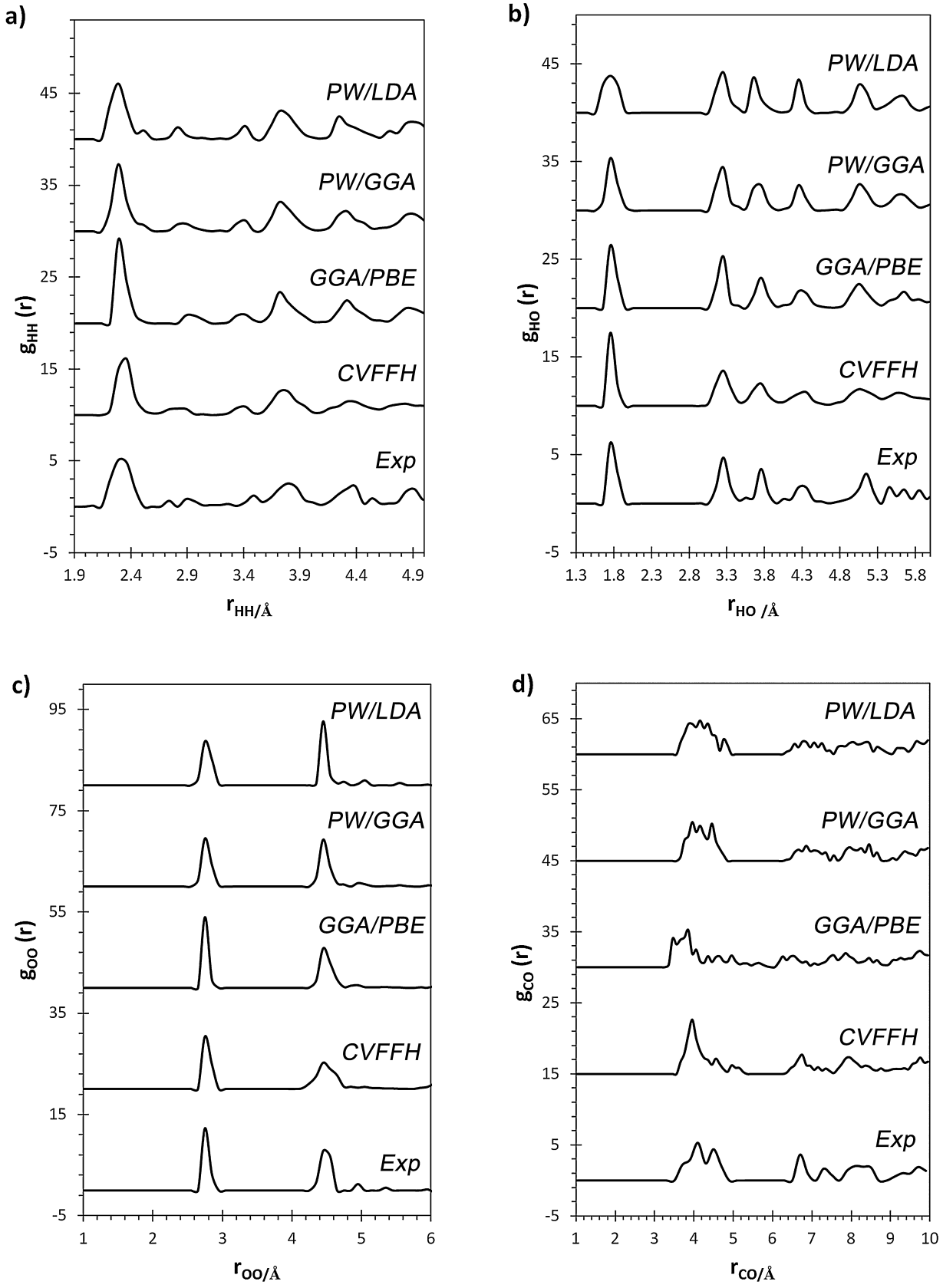

Fig. 3. RDFs of HH (a), OH (b), OO (c), and CO (d) atoms of the crystal lattice of methane hydrate optimized at constant volume with different methods comparing with experimental structure.

Table 3
Crystal lattice parameters of methane hydrate fully optimized with variable volume with different theoretical methods and comparison with experimental data (distances in Å and angles in°).

Features	Exp[a]	GGA[b]	PW/GGA[c]	PW/LDA[d]	CVFFH[e]
a (Å)	11.95 (11.88)	11.91 (11.59)	11.56	10.87	11.83
b (Å)	11.95 (11.88)	11.94 (11.60)	11.58	10.86	11.42
c (Å)	11.95 (11.88)	11.98 (11.56)	11.57	10.85	11.37
α (°)	90.0	90.1 (89.8)	90.0	90.1	88.6
β (°)	90.0	90.2 (90.6)	90.2	90.3	88.6
γ (°)	90.0	89.9 (90.1)	89.9	90.1	91.2

[a] From experimental structure obtained from X-ray diffraction [61]; values in brackets were reported by Kirchner et al. [68].
[b] Optimized with SIESTA and RPBE parameterization (values in brackets are using PBE).
[c] Calculated with plane-waves using CASTEP.
[d] Calculated with plane-waves using CASTEP, $E_{cut\text{-}off}$ = 700 eV.
[e] Calculated with CVFFH force field.

similar to those recently reported using DFT calculations with van der Waals interactions implemented in the functional [19].

Similar behavior was obtained in the calculations of CO_2 hydrate crystal lattice at variable volume (a = 11.75–11.92 Å, 11.39–11.78 Å with GGA/PBE and CVFFH calculations respectively) being consistent with experimental neutron diffraction values (a = 11.81–11.89 Å) [66].

2.3. Gas occupancy in hydrates

2.3.1. Encapsulation energies

Taking into account the weakness of the intermolecular interactions existing in these clathrates, different theoretical methods are compared for calculating the encapsulation energy that is the binding energy of gas-guest into the clathrate cage. Binding energy of one methane molecule inside an isolated 5^{12} cage was calculated initially using the cluster model. In general, the formation of this clathrate is exothermic with negative energy values with HF (-5.38 kcal mol^{-1}), CVFFH (-5.19 kcal mol^{-1}) and LDA (-7.59 kcal mol^{-1}) methods, being close to previous MP2 calculations (-6.1 kcal mol^{-1}) [69]. These methods yield binding energies in a similar range, although LDA yields a slightly higher energy due to the shrinking effect of the optimization with this method with shorter interatomic distances in the cage. However, the GGA/PW method yields a binding energy of +1.97 kcal mol^{-1}, being significantly different to those of other methods. These results show that GGA is not an appropriate method for describing such weak interactions. This is consistent with previous calculations of systems with weak interactions like the adsorption of aromatics on phyllosilicate surface [58]. Previous dispersion-corrected DFT (DFT-D) calculations yielded a binding energy of -6.9 kcal mol^{-1} that is in the same range of our results [70]. Recent studies of similar cluster model of this clathrate compared the binding energy of the guest methane molecule with the host water cage calculated with different methods including long-range corrected functionals and DFT-D methods yielding values in the range of 4.4–6.87 kcal mol^{-1}, however the best methods describing van der Waals interactions overestimated the hydrogen bonding of the water molecules [17]. Finally, they chose a DFT-D method yielding a binding energy of 5.25 kcal mol^{-1} [18]. Nevertheless, these results are also close to our values.

In the isolated 5^{12} cage of the CO_2 hydrate cluster model the calculated binding energy is slightly more exothermic (-5.52 kcal mol^{-1} and -6.68 kcal mol^{-1} with HF and CVFFH, respectively) than in methane hydrate.

The encapsulation energy for the whole hydrate crystal calculated with CASTEP/LDA is -47.23 kcal mol^{-1} per unit cell corresponding to 8 methane molecules per methane hydrate unit cell. Then the binding energy per methane molecule is -5.90 kcal mol^{-1}. The same calculation was made with CVFFH resulting an encapsulation energy of -48.88 kcal mol^{-1} for 8 methane molecules within the unit cell, which means -6.11 kcal mol^{-1} per methane molecule. Both methods yield similar energy values and in the same range that those obtained with the one cage cluster model. This energy value seems to be a certain high for only weak van der Waals interactions and the existence of some additional electrostatic forces, corroborated by spectroscopic properties (see later), could justify the high binding energy value. Recently, DFT calculations with van der Waals corrections yielded higher binding energy values (-11.8 kcal mol^{-1}) for this system [16]. However, this value is close to the experimental binding energy of water on mica surface where stronger electrostatic and hydrogen bond interactions are present [71]. Therefore, we consider that this value previously reported is overestimated and too high for weak van der Waals interactions comparing with our values and previous calculations with a wide series of long-range corrected functionals and DFT-D methods [17,18,70].

We calculated binding energies of different number of methane molecules within the hydrogen bonding network that composes crystalline structure of clathrate by using CVFFH. We found that in the crystal lattice of hydrate the binding energy of only one methane molecule located inside a small cage (5^{12}) is higher, -6.25 kcal mol^{-1}, than in a large ($5^{12}6^2$) cage, -5.69 kcal mol^{-1}. Similar behavior was found with DMol^3/LDA calculations. Methane hydrate crystal with a complete occupancy has six methane molecules inside large cages and two methane molecules in small cages. Hence taking into account this population and the binding energy of each cage, the weighted average value is lower (-5.83 kcal mol^{-1}) than the energy per methane molecule in a lattice crystal with complete occupancy (-6.11 kcal mol^{-1}). Calculations filling the hydrate crystal with a progressive number of methane molecules were performed. Calculations of the crystal lattice of hydrate with two guest molecules, one methane in each kind of cages, yielded average binding energy of -6.05 kcal mol^{-1} per methane molecule. This is very close to the average value for the crystal lattice with full occupancy. Increasing the methane occupancy in the crystal lattice of hydrate in the large $5^{12}6^2$ cages surrounding one small cage occupied gives average binding energies of -6.25 kcal mol^{-1}, -6.05 kcal mol^{-1}, -5.95 kcal mol^{-1}, -5.96 kcal mol^{-1}, -5.98 kcal mol^{-1}, -6.00 kcal mol^{-1}, and -6.11 kcal mol^{-1} for 1 (in small cage), 2 (one in small cage and one in large cage), 3 (one in small cage and 2 in large cages), 4, 5, 6, 7 (one in small cage and 6 in large cages), and 8 methane molecules, respectively. This shows that the effect of the occupancy in large cages slightly increases the binding energy of methane in the hydrate. It means that there is some stabilizing interaction between the methane molecules and the walls of cages in small and large cages.

Previous experimental Raman spectroscopy studies found that the formation of the large cages from liquid water can be the rate

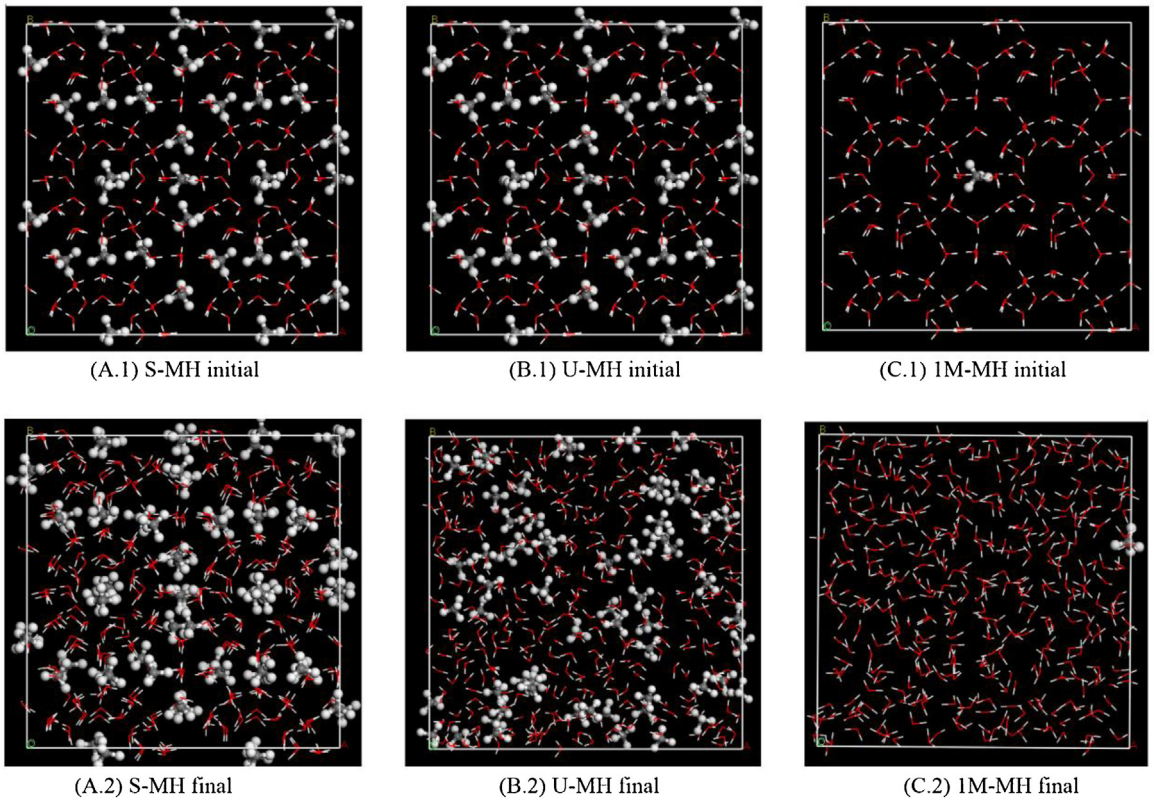

Fig. 4. Snapshots of initial and final configurations of methane hydrate crystal lattice in the MD trajectories.

limiting during sI methane hydrate formation and larger number of 5^{12} cages than $5^{12}6^2$ cages was observed [72]. Moudrakovski et al. [73] using hyperpolarized ^{129}Xe NMR spectroscopy studies has also shown that more 5^{12} cages are present in the early stage of hydrate formation formed from ice. These results can be explained by the higher binding energy of methane in the small cage than in the large one found by us. Our results contrast with recent van der Waals DFT calculations [16] that obtained too high binding energy values being higher for $5^{12}6^2$ cages (-13.6 kcal mol^{-1}) than for 5^{12} cages (-12.0 kcal mol^{-1}), the opposite to the experimental results. However, other experimental studies found that the occupancy in large cages is higher than in small ones [42]. These discrepancies can exist because the binding energy differences between large and small cages are not significant and probably entropic or kinetic aspects can vary the relative occupancy in each case.

In the fully occupied CO_2 hydrate crystal lattice, the binding energy for 8 molecules of CO_2 per unit cell is -40.34 kcal mol^{-1}, which is lower than in the fully occupied methane hydrate crystal. However, the binding energy of only one CO_2 molecule per unit cell is -8.24 kcal mol^{-1} and -9.23 kcal mol^{-1} in the 5^{12} and $5^{12}6^2$ cages, respectively. In this clathrate the adsorption in the large cage is more exothermic than in the small one, and the full occupancy of CO_2 is not favorable being mainly in the large cages, according with experimental behavior where the occupancy of CO_2 in the large cages is more likely than in the small ones [65].

2.3.2. Molecular dynamics simulations

For these simulations a $2 \times 2 \times 2$ supercell of the crystal lattice of hydrate was generated with periodic boundary conditions with full occupancy and with only one methane molecule in one small cage. NPT ensemble molecular dynamics (MD) simulations were performed with CVFFH force field at different conditions: At pressure $P = 40$ bar and temperature $T = 273$ K for hydrate fully occupied under stable conditions (S-MH); at $P = 40$ bar and $T = 370$ K for hydrate fully occupied under unstable conditions (U-MH); and at $P = 1$ bar and $T = 400$ K for hydrate with only one methane molecule in small cage (1M-MH). The temperature and pressure of the model system are controlled using Andersen [74] and Berendsen [62] methods, respectively; and these values are high enough to accelerate the process and to observe the dynamics of the system at different extreme conditions, they do not try to reproduce the experimental values of state-change which are out of the scope of this work. The van der Waals and long-range Coulomb interactions are calculated with the Ewald summation. All simulations were carried out during 100 ps with a time step of 1 fs.

Snapshots of the MD trajectories (Fig. 4) for S-MH show that methane hydrate structure keeps stable with the disordering of the methane molecules due to their rotation in the cages without significant distortions of hydrogen bonding network. This was maintained even at longer simulations (200 ps). However, in U-MH the hydrogen bonding network is collapsed and can be observed that methane molecules tend to form aggregates. The model with only one methane molecule was created to observe the displacement of methane molecule through the cages that composes hydrate structure when it starts to destabilize. The 1M-MH model is used to explore the diffusion of methane through the hydrate crystal. In 1M-MH, it can be observed that during the trajectory the hydrogen bonding network is completely disordered, when methane molecule tries to diffuse from the small cage to another cage.

RDF profiles of O–O atom-pairs, g_{OO}, display a common maximal peak at $r_{OO} = 2.8$ Å, corresponding to the nearest distance between H_2O molecules joined by hydrogen bonds in S-MH, U-MH and 1M-MH (Fig. 5a). In S-MH other maximal peaks appear at $r_{OO} = 4.6$ Å and 6.5 Å, respectively, corresponding to farther vicinal H_2O molecules in hydrates. Our RDF (O–O) profiles are consistent with previous MD simulations [75]. These peaks are not observed in U-MH and 1M-MH, because methane hydrate crystal structure is not maintained and it becomes disordered. Only the first peak at 2.8–3.0 Å

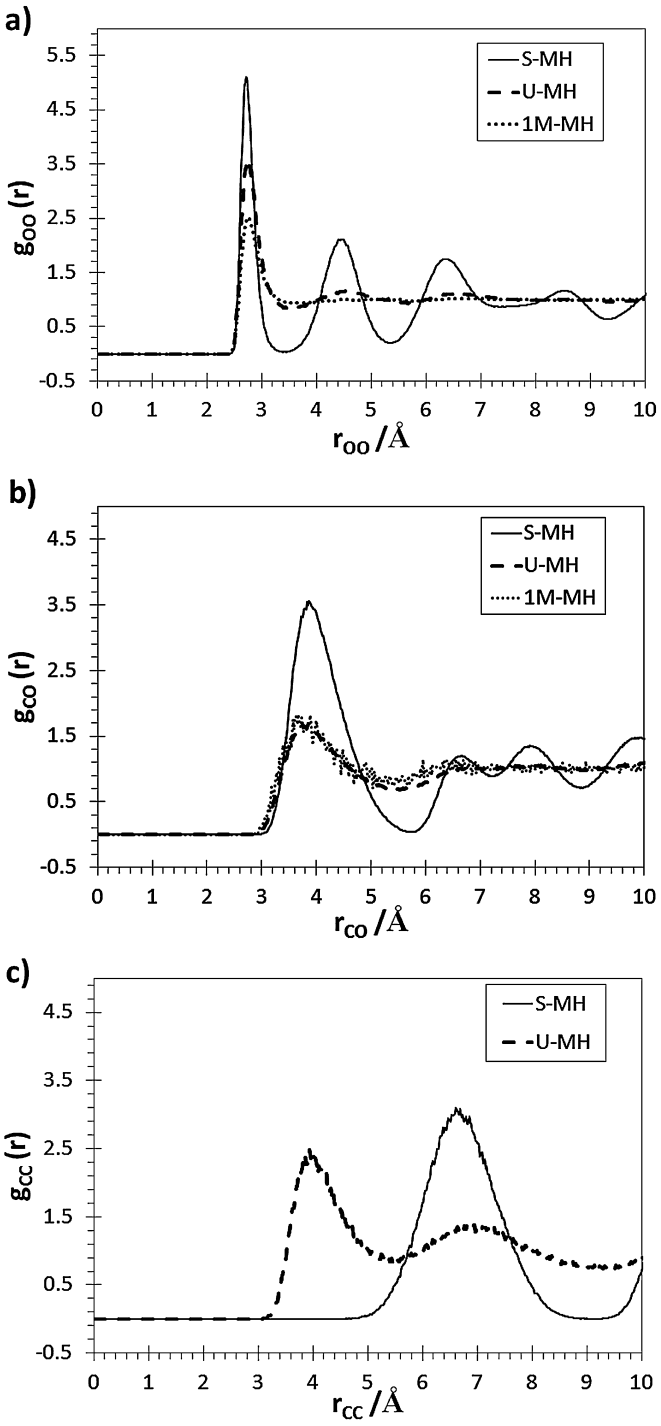

Fig. 5. RDF profiles of OO (a), CO (b) and CC (c) atoms in methane hydrate crystal structure obtained from MD simulations. S-MH (solid line), U-MH (dash line), and 1M-MH (dot line).

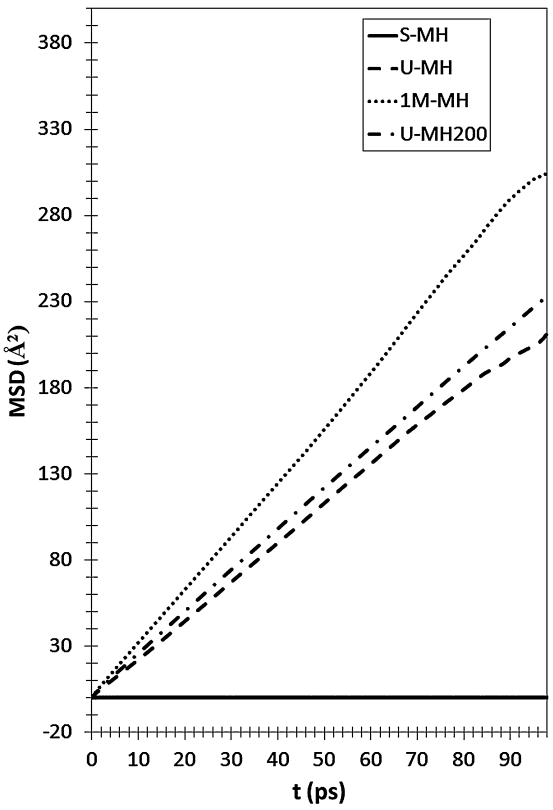

Fig. 6. MSD of water molecules in methane hydrate obtained from MD simulations. The solid line represents the methane hydrate under stable conditions (S-MH). The methane hydrate under unstable conditions (U-MH) is described by a dash line (MD of 100 ps) and dot-dash line (MD of 200 ps). The diffusion for only one methane in the hydrate is represented by a dot-line.

is maintained with a certain tail corresponding to the vicinal water molecules forming H bonding as observed in liquid water (Fig. 2). In the RDF profiles of C and O atoms, g_{CO}, a maximal peak around r_{CO} = 4 Å remains in all three MD simulations corresponding to the water molecules surrounding the methane. However, in the disordered structures, U-MH and 1M-MH, this maximal peak are more broad and the maximum appears at shorter distances (3.5–3.8 Å) than in S-MH (3.9–4.0 Å), indicating that the C–O distances are slightly shorter than in the crystal structure and close to those of liquid solvated methane. This is consistent with experimental neutron diffraction studies on methane hydrate formation [67]. Besides, the rest of the g_{CO} peaks at 6.6 Å, 8.0 Å, and 9.8 Å of the crystal lattice of hydrate remains only in S-MH corresponding to the long-range order of the crystal structure. On the other hand, the RDF peaks of C atoms in CH_4 molecules, g_{CC}, appears at r_{CC} = 3.4–4.6 Å and 6–8 Å as very broad peaks in U-MH, whereas only one peak at 6.8 Å appears in S-MH, showing that with rising temperature, methane hydrates become less stable, and methane molecules tend to be aggregate with shorter CC distances than in the crystal lattice, this is consistent with previous computational studies [27,28,75].

The mean square displacement (MSD) is a measure of the average distance that a molecule travels during simulations. For a system at equilibrium, the particles will move in accordance with the equations of motion that define the system and, in general, will tend to diffuse away from their original location. For a stable crystal, the constituent atoms vibrate around their sites in the crystal lattice without diffusing. Fig. 6 illustrates MSD profiles of H_2O molecules in the CH_4 hydrate. In S-MH MSD shows a typical solid profile without diffusion, while in U-MH the slope is higher and the H_2O molecule diffusion occurs easier (similar behavior was observed with longer MD simulations at 200 ps). In 1M-MH the MSD is slightly higher than in U-MH implying disorder and loss of crystalline structure. Based on MSD profiles, the water diffusion coefficients were calculated, yielding 0.366 (0.355 with MD of 200 ps) $Å^2\ s^{-1}$ for U-MH; 0.531 $Å^2\ s^{-1}$ for 1M-MH; and 5×10^{-6} $Å^2\ s^{-1}$ for S-MH. Peters et al. [76] found that water vacancies or defects are necessary in the clathrate structure for producing the CH_4 diffusion along the crystal as a rather rare event.

Optimizing at variable volume the disordered U-MH and the ordered S-MH structures of hydrate sampled from the above molecular dynamics simulations after a final equilibration; we found that

the crystal lattice is much more stable in 81.4 eV/per-unit-cell than the disordered phase, which seems to be more likely a methane dissolution than an amorphous hydrate. This means that the crystallization of methane hydrate is an exothermic process. This fact and our molecular dynamics simulations study indicate that the crystallization of methane hydrate requires several steps. First the methane dissolution in water forms small aggregates solvated by water molecules and special conditions of pressure and temperature are necessary to disperse maximally the methane molecules in the water solution. The presence of the hydrophobic interactions of each methane molecule with the surrounding water molecules facilitates the formation of the hydrate crystal under these conditions. When the methane hydrate crystal is formed, no diffusion of methane is possible through the crystal cages.

Our results from 1M-MH and U-MH simulation trajectories show that there is no preferential methane hydrate decomposition depending on the nature of cages. This is consistent with previous Molecular Dynamics studies [28,77] and with experimental results based on NMR spectroscopy [73,78], where the time-resolved methane hydrate dissociation data showed that the hydrate occupancy ratio remained constant during dissociation. The constant occupancy ratio suggested that the unit cell of sI methane hydrate was dissociated as a whole as shown in our simulations.

In order to explore the diffusion of methane through the hydrate crystal, we optimized two models of the crystal structure of clathrate with only one methane molecule: one with the methane in the small cage, and the another one with the methane in the large cage by DMol^3/DFT calculations. We searched a TS along the trajectory path between both models and we found a saddle point of the potential energy surface for the transition of the methane molecule from the small to the large cage yielding a large energy barrier (188.6 kcal mol^{-1}) confirming the above results. However, we generated one defect in the crystal structure, creating a vacancy of one water molecule in the bridging wall between the vicinal small (5^{12}) and large ($5^{12}6^2$) cages. With this new model, we optimized two new models with only one methane molecule: one with methane in the small 5^{12} cage, and another one with the methane in the large $5^{12}6^2$ cage and we explored the transition path of the methane molecule from the small to the large cage. We found a TS for this transition with a energy barrier of 5.47 kcal mol^{-1}. This barrier is significantly lower than that in a complete clathrate crystal. Therefore, this result confirms our above conclusions and those previously reported where some defects are necessary to allow the diffusion of methane molecules through the hydrate crystal [76].

2.3.3. Vibration spectroscopic properties

Vibration spectroscopy can be useful to distinguish the frequencies of the $\nu(CH)_s$ modes of this methane clathrate. However, one of the scientific challenges related with clathrate hydrates is the anomalous shift in the stretching vibration frequency of methane molecules in the clathrate with respect to that in gas phase. Experimentally it was observed that the $\nu(CH)_s$ mode of the methane in the large cage shifts to lower frequency than that in small cage. But this estimation was based only on peak intensities and apparently this is opposite of that it was expected where the guest-host interactions in the large cage are weaker than in the small cage. However, the frequency shifts are very small and some differences are found in literature: Sum et al. [32] assigned these $\nu(CH)_s$ bands to 2905 (large cage) and 2915 (small cage) cm^{-1}, whereas Ohno et al. [37] proposed to 2901 cm^{-1} and 2914 cm^{-1}, and Tulk et al. [33] reported 2904 cm^{-1} and 2916 cm^{-1}, respectively. Besides, some discrepancies have been reported in the assignments of these bands, where Seitz et al. [41] and Hester et al. [42] reported the opposite assignments with respect to those of Sum et al. [32], Tulk et al. [33] and Ohno et al. [37]. Hence, it is necessary to understand deeply the origin of this phenomenon from an atomistic point of view. Previous authors have demanded the necessity of applying quantum-mechanical calculations to this field [33,53] and recently frequencies calculated from ab initio molecular dynamics have been reported [20]. The present study reports some calculations related to this question.

The vibration frequencies of methane were calculated using different methods and configurations of methane molecule, at gas phase, in a cluster of the small 5^{12} cage of clathrate, in a model of the $5^{12}6^2$ cage of clathrate, and in a crystal lattice of methane hydrate (Table 4). For a free methane molecule at gas phase, calculations were made using HF (HF/6-311G**), MP2 (MP2/6-311G**), SIESTA (GGA/PBE, $E_{cut\text{-}off}$ = 550 Ry) and CVFFH force field. Comparing with experimental data [79], no correlation was found between the CVFFH results and experimental frequencies. Using quantum–mechanical methods, in general, the calculated absolute values of frequencies are higher than experimental ones due to the lack of anharmonicity in the calculations. However, linear relationships between calculated and experimental frequencies were found with scale factors of 0.923 (HF, correlation coefficient R = 0.994), 0.948 (MP2, R = 0.999), and 0.946 (SIESTA, R = 0.997). Hence, our quantum–mechanical calculations are consistent with experimental frequencies (Table 4).

In order to obtain vibration frequencies of methane hydrates using quantum-mechanical methods, geometry optimizations of clusters composed of small and large cages were performed along with vibration frequencies. The optimization of the large cage cluster converged only with the HF method. Hence we used only the HF method for comparing the calculated frequencies of the hydrate with the experimental ones, finding a linear relationship with a scale factor of 0.9214. The vibration modes of the water molecules making up the host lattice appear experimentally within the range of 3100–3700 cm^{-1}, although it is not easy to distinguish the vibrations of the water molecules of the methane hydrate crystal from those of ice [33]. Our calculated values fit within the experimental range.

In agreement with the assignment of symmetric methane C–H stretching, ν_s(C–H), peak made by previous experimental Raman studies [37], our results with HF calculations shows a high frequency peak (2920 cm^{-1}) corresponding to small cages, and a low frequency peak (2901 cm^{-1}) that corresponds to large cages of methane hydrate. The calculated frequencies of ν_{as}(C–H) are consistent with the experimental values [33]. The δ(CH) modes appear at similar frequencies for both kinds of cages being only slightly higher than in gas phase. No experimental data of these modes was found hence our data can be used for future experimental assignments for these modes.

In our calculations on hydrate crystal lattice based on SIESTA no clear differences were distinguished between the methane in small and large cages due to the high degree of coupling between the atomic vibrations of the methane molecules in the clathrate crystal. Nevertheless a linear relationship was found with experimental data with a scale factor of 0.956, finding values close to the experimental range. However, the behavior in ν_s(C–H) modes is the opposite of our above results and the main experimental assignments, appearing at slightly higher frequency those of large cages than those of small cages. Probably the limitations of these SIESTA calculations are in the use of pseudopotentials for describing properly the electrostatic interactions between atoms during the vibration mode movement. This misfitting can give us a constructive idea confirming that the origin of the frequency difference in ν_s(C–H) of small and large cage is not owing to the electronic structure of methane and water molecules but owing to the local electrostatic interactions between the H_m atoms and the water molecules of clathrates in the atomic movement of the vibration mode.

Table 4
Calculated frequencies (cm^{-1}) of the main vibration modes of the methane molecules at gas phase and within the clathrate comparing with experimental values.

Phase	Method[a]	υ_{as}(C–H)	υ_{s}(C–H)	δ(C–H) (rock)	δ(C–H) (umbrella)
Molecule	Exp.	3019, 3022[b]	2917	1534	1306
	HF	3007	2911	1539	1340
	MP2	3044	2914	1499	1294
	SIESTA	3042	2933	1516	1234
Small cage cluster	HF	3021	2920	1548	1352
	SIESTA	3060	2920	1513	1266
Large cage cluster	HF	3008	2901	1550	1352
Crystal lattice hydrate	Exp	3053[b], 3026[c]	2914[d,e], 2901–2903[d,f]		
	SIESTA	3060–3031	2906[e], 2914[f]	1439[e], 1505[f]	1251[e], 1258[f]
	CVFFH	3078[e], 3070[f]	2914[e], 2903[f]	1638[e], 1634[f]	1461[e], 1456[f]

[a] Exp. means experimental data [79], HF is HF/6-311G** level, MP2 is MP2/6-311G** level, SIESTA refers to DFT calculations based on atomic basis sets and GGA/PBE level.
[b] Raman spectroscopy experimental data from Chazallon et al. [35].
[c] Raman spectroscopy experimental data from Tulk et al. [33].
[d] Raman spectroscopy experimental data from Ohno et al. [37].
[e] Assigned to the methane in small cages.
[f] Methane in large cages.

Our calculations of the crystal lattice of hydrate with CVFFH yield values close to the experimental range with a linear relationship and a scale factor of 1.076. In these calculations the methane molecules can be distinguished by the frequencies of their vibration modes according with previous force field calculation [29]. We reproduce the experimental relative behavior in ν_s(C–H) where its frequency for small cages (2914 cm^{-1}) is higher than in large cages (2903 cm^{-1}). Similar differences were found in previous calculations although with different values (2871 cm^{-1} and 2863 cm^{-1} for small and large cages, respectively [20]; and 3014 cm^{-1} and 2967 cm^{-1} for small and large cages, respectively [53]) to the experimental ones. Our calculated ν_{as}(C–H) frequencies are consistent with previous simulations [30] and also the frequency for small cages (3078 cm^{-1}) is higher than in large cages (3070 cm^{-1}). Similar differences were found in previous calculations and our values are in the balance between the previous ones (3167–3152 cm^{-1} [53], and 2976–2960 cm^{-1} [20] for small-large cages, respectively).

In the small cage the interactions between the methane molecule and the water OH groups are stronger than in the large cage and the ν(C–H) mode appears at higher frequency. Similar effect was observed in the adsorption of formic acid on silicate surface, where a high-frequency shift occurred in the ν(C–H) mode due to the interactions of CH groups with the SiOH groups [80]. In small cages the methane is closer to the water molecule like in the aqueous solution of methane where the methane molecules is surrounded by water molecules and the $\nu(CH)_s$ mode appears at 2911 cm^{-1}, close to the frequency of the methane in small cage [72].

Some authors have explained this phenomenon with the Charles-Pimentel model, loose cage-tight cage [81], the existence of local minima of the guest molecule inside the hydrate cage that enhance host–guest interactions. However, this cannot explain the fact that the frequencies of clathrate are lower than those of a free methane molecule and experimental techniques showed that there is no local minimum of the guest molecule orientation in the cages [53]. Another explanation is that this frequency difference is due to a perturbation of the local electrostatic fields produced by the water molecules of the cage walls [35]. This is reasonable but it is a general explanation because the electrostatic interactions will be lower when the guest–host distance increases and the frequency in large cage would be closer to that of free molecule the opposite to that observed. Nevertheless, this explanation can be accepted with a further detail. When the methane is confined in the cage, the C–H bond is surrounded by an electric field and the stretching atomic movement has to overcome this electric field increasing the force constant and then increasing the frequency. Hence the frequency will be higher in the small cage than in the large cage. This effect is not specific of methane clathrate but is more general like we observed high frequency shift of C–H group interacting with OH groups in previous studies [80]. However, in the hydrate cages these frequencies are lower than in the free molecule. This indicates that an additional force is involved during this vibration mode. In both cages, the methane H atoms are oriented towards the O atoms of water molecules of the cage walls producing an attractive electrostatic interaction decreasing the force constant of the stretching vibration, and then decreasing the frequency. On the other hand, in the small cage, our calculations show that the H_m...H distances are smaller than the H_m...O distances and also repulsive electrostatic interactions occur. In this small cage the effect of the electric field is strong and will balance the attractive effect, maintaining the frequency close to that of free molecule. However, in the large cage the electric field is lower because the distance are slightly longer and the guest molecule will have more rotation freedom allowing to H atoms to be better oriented towards the O atoms increasing the attractive effect and then decreasing the frequency. This explanation is supported by our calculations that find a slightly longer C–H bond length for the methane molecule of the large cage than in that of small cage according with previous results [53]. This slight difference will yield a lower force constant and a lower frequency for a stretching vibration mode as found in the large cage.

The vibration spectroscopy is also interesting for assessment of the presence of CO_2 hydrates, however some uncertainties are found in literature, some overtones of bending modes are considered as stretching normal modes [41] and only the occupancy in large ($5^{12}6^2$) cages has been reported in many cases [82]. In our CO_2 hydrate models the vibration frequencies were also calculated in the 5^{12} and $5^{12}6^2$ cages models and in the crystal lattice and compared with the isolated CO_2 gas molecule and experimental data (Table 5). A linear relationship was also observed between the calculated and experimental values finding a constant scale factor, 0.96 for MP2 values ($R = 0.9999$), 0.89 for HF values ($R = 0.9986$), and 0.977 ($R = 0.9999$) for Siesta values. For free CO_2 molecule, the values calculated with MP2 and SIESTA methods are closer to experimental one than those from HF calculations. Then we can consider the SIESTA studies for the clathrate structures. In the crystal lattice of CO_2 hydrate, the frequencies of all normal modes are lower than those of the free molecule according with the experimental behavior [36,39]. Besides, small differences in frequency are found between the CO_2 molecules in the small 5^{12} cage and large $5^{12}6^2$ cage. Frequencies of stretching modes of CO_2 in small cages are higher than in the large cages. However, the opposite is observed in the bending mode of CO_2. Experimentally two bands of asymmetric stretching mode of CO_2 have been detected but no clear frequency difference has been reported [36].

Table 5
Calculated frequencies (cm^{-1}) of the main vibration modes of the CO_2 hydrate in small and large cages, in the crystal lattice and as an isolated molecule at gas phase comparing with experimental values.

Phase	Method[a]	υ_s(C–O)	δ_s(C–O)	ν_{as}(C–O)
Molecule	Exp.	1285[b]	667[c]	2349[c], 2345[d]
	HF	1355	683	2307
	MP2	1288	632	2359
	SIESTA	1289	637	2355
Small cage cluster	HF	1366	674	2321
	SIESTA	1273	606	2284
Large cage cluster	HF	1364	683	2316
	SIESTA	1263	627	2269
Crystal lattice hydrate	Exp	1275[b]		2347[e], 2335[e]
	SIESTA	1276[f], 1267[g]	611[f], 624[g]	2287[f], 2273[g]

[a] Exp. means experimental data, HF is HF/6-311G** level, MP2 is MP2/6-311G** level, SIESTA refers to calculations based on atomic basis sets and GGA/PBE level.
[b] Experimental data from Beeskow-Strauch et al. [82].
[c] Experimental data from Lide [79].
[d] Experimental data from Prasad et al. [39].
[e] Raman spectroscopy experimental values from Dartois and Schmitt [36].
[f] Assigned to the CO_2 in small cages.
[g] CO_2 in large cages.

3. Conclusions

Crystalline structure of hydrates of CO_2 and methane can be successfully reproduced using computational methods based on DFT (SIESTA, CASTEP) and using empirical interatomic potentials (CVFFH). The inclusion of quantum mechanical calculations has been demanded by previous authors [33,53]. Comparing lattice parameters on calculations at variable volume, best results are obtained with SIESTA and the CVFFH force field.

Calculated binding energies of methane molecules into the hydrate clathrate cages yield negative values, except for CASTEP with GGA approximation, proving that GGA is not an appropriate method for such weak interactions. Those negatives values prove that methane hydrate formation is an exothermic process ($-6.11\,kcal\,mol^{-1}$ per methane molecule). These energy values can correspond to the van der Waals interactions between adsorbate and clathrate water molecules, although they are high for only dispersion interactions ($-2.7\,kcal\,mol^{-1}$ for benzene dimer) [83]. The methane molecule is confined in a limited zone with a smaller size than the molecular volume taking into account the van der Waals radii. On the other hand, the methane molecule can be considered as a positively charged shell of H atoms, surrounding a negatively charged C atom. Therefore, additional electrostatic interactions between methane and water molecules into the confined space of the clathrate cage can justify this binding energy value.

The CVFFH force field describes reasonably well these interactions since it is parameterized including van der Waals interactions. Conventional semilocal DFT functionals describe dispersive attraction very poorly. However the LDA method describes also well these interactions though it mimics the van der Waals attractions being the result of an error cancellation with the missing electron correlation and the short range overbinding effects [84]. Recent calculations including the van der Waals forces into the DFT functionals have reported too high binding energies for this system ($-12\,kcal\,mol^{-1}$). Therefore, this methane hydrate crystal system can be a good benchmark example for the improvement of DFT methods to describe the dispersion and electrostatic forces existing in a locally charged confined space, out of the scope of this work, in further investigations. A great similarity in structure and relative energies is observed in the CO_2 hydrate with the methane hydrate crystal.

A comparison of the binding energy indicates that the methane molecule in small cages (5^{12}) of the hydrate crystal is more stable than in large cages ($5^{12}6^2$). This fact is consistent with the hypothesis of considering the isolated small cages as precursors of formation of methane hydrate where in the aggregation and assembly of the small cages forming the crystal structure, the large cages appear. Our calculations found a certain stabilizing interaction between the inner methane into the small cage and external methane molecules. Hence the small cages can be surrounded by dispersed methane molecules. These external methane molecules with additional small cages and water molecules can form an amorphous proto-crystalline hydrate. This amorphous hydrate will give enough fugacity to the methane molecules for diffusion and reaching the high occupancy of the most large and small cages. This high occupancy and the size of the amorphous particle will help to be ordered and nucleate a crystal. This conclusion is consistent with previous interpretations [23]. Nevertheless, the binding energy differences are very small between small and large cages and other entropic and kinetic effects can change the adsorption and the relative occupancy in the crystal lattice.

Molecular Dynamics simulations shows that under conditions of stability, crystalline structure of methane hydrate remains, but rising temperature methane hydrate decomposes, disordering the hydrogen bonding network, and methane molecules tend to be aggregate. MD with just one methane molecule in small cage shows that when rising temperature, methane diffuses once the hydrogen bonding network is been collapsed, and therefore, the diffusion of methane from a small to a large cage, cannot be reproduced. However, the presence of defects of water molecules in the crystal lattice can facilitate significantly the diffusion of methane molecules. Hence, methane molecules will not diffuse into the hydrate once the crystal structure of methane hydrate is formed, and only they will be able to diffuse before in an amorphous precursor. This indicates that the replacement of CO_2 in the methane hydrate clathrate to produce CO_2 hydrate clathrate and free methane should involve a dissociation and recrystallization of the hydrate crystal lattice.

The vibration stretching peaks of C–H at $2915\,cm^{-1}$ and $2905\,cm^{-1}$ are due to small and large cages respectively, so the vibration behavior of methane molecules in small cages is similar to that of methane gas. No complete explanation has been reported yet because previous authors were searching simple interactions. We found that the combination and balance of opposite forces (repulsive forces between H atoms and attractive forces between H and O atoms) between the methane and water molecules within the cages of the hydrate crystal can justify the frequency differences of the methane molecule in small cage, in large cage and in gas phase.

Acknowledgements

Funding for this work came from Junta de Andalucía RNM-3581 CADHYS project. Authors are thankful to H. Heinz for his useful discussions and for facilitating the force fields, M. V. Fernández-Serra, M. Pruneda for their useful discussions, W. Kuhs for the availability of crystal atomic data of methane hydrate, and to the Junta de Andalucía for the financial support, to the Supercomputational Center of the Granada University (UGRGRID), to the Centro Técnico de Informática del CSIC.

References

[1] E.D. Sloan, Geol. Soc. Lond. Spec. Publ. 137 (1998) 31.
[2] M.K. Davie, O.Y. Zatsepina, B.A. Buffett, Mar. Geol. 203 (2004) 177.
[3] A.V. Milkov, Org. Geochem. 36 (2005) 681.
[4] J.B. Klauda, S.I. Sandler, Energy Fuels 19 (2005) 459.
[5] B.A. Buffet, D. Archer, Earth Planet. Sci. 227 (2004) 185.
[6] K.A. Kvenvolden, B.W. Rogers, Mar. Petrol. Geol. 22 (2005) 579.
[7] J.P. Kennett, K.G. Cannariato, I.L. Hendy, R.J. Behl, Methane Hydrates in Quaternary Climate Change: The Clathrate Gun Hypothesis, American Geophysical Union, Washington, DC, 2003.
[8] N. Shakhova, I. Semiletov, A. Salyuk, V. Yusupov, D. Kosmach, O. Gustafsson, Science 327 (2010) 1246.
[9] D. Archer, Biogeosci. Discuss. 4 (2007) 993.
[10] R. Boswell, Science 325 (2009) 957.
[11] S. Machida, H. Hirai, T. Kawamura, Y. Yamamoto, T. Yagi, Phys. Earth Planet. Inter. 155 (2006) 170.
[12] A. Germinale, V. Formisano, M. Giuranna, Planet. Space Sci. 56 (2008) 1194.
[13] E. Chassefiere, Icarus 204 (2009) 137.
[14] Q. Du, P. Li, P. Liu, R. Huang, J. Mol. Graph. Model. 27 (2008) 140.
[15] R. Sun, Z. Duan, Geochim. Cosmochim. Acta 69 (2005) 4411.
[16] G. Román-Pérez, M. Moaied, J.M. Soler, F. Yndurain, Phys. Rev. Lett. 105 (2010) 145901.
[17] Y. Liu, J. Zhao, F. Li, Z. Chen, J. Comput. Chem. 34 (2013) 121.
[18] L. Tang, Y. Su, Y. Liu, J. Zhao, R. Qiu, J. Chem. Phys. 136 (2012) 224508.
[19] Q. Li, B. Kolb, G. Román-Pérez, J.M. Soler, F. Yndurain, D.C. Langreth, T. Thonhauser, Phys. Rev. B 84 (2011) 153103.
[20] M. Hiratsuka, R. Ohmura, A.K. Sum, K. Yasuoka, J. Chem. Phys. 136 (2012) 44508.
[21] V. Chihaia, S. Adams, W.F. Kuhs, Chem. Phys. 317 (2005) 208.
[22] M. Rodger, Ann. N. Y. Acad. Sci. 912 (2000) 474.
[23] L.C. Jacobson, H. Waldemar, V. Molinero, J. Am. Chem. Soc. 132 (2010) 11806.
[24] J. Vatamanu, P.G. Kusalik, Phys. Chem. Chem. Phys. 12 (2010) 15065.
[25] S. Liang, P.G. Kusalik, Chem. Phys. Lett. 494 (2010) 123.
[26] C. Moon, P.C. Taylor, P.M. Rodger, J. Am. Chem. Soc. 125 (2003) 4706.
[27] S.A. Bagherzadeh, P. Englezos, S. Alavi, J.A. Ripmeester, J. Chem. Thermodyn. 44 (2012) 13.
[28] E.M. Myshakin, H. Jiang, R.P. Warzinski, K.D. Jordan, J. Phys. Chem. A 113 (2009) 1913.
[29] J.A. Greathouse, R.T. Cygan, B.A. Simmons, J. Phys. Chem. B 110 (2006) 6428.
[30] H. Itoh, K. Kawamura, Ann. N. Y. Acad. Sci. 912 (2000) 693.
[31] H. Jiang, K.D. Jordan, C.E. Taylor, J. Phys. Chem. B 111 (2007) 6486.
[32] A.K. Sum, R.C. Burrus, E.D. Sloan Jr., J. Phys. Chem. B 101 (1997) 7371.
[33] C.A. Tulk, J.A. Ripmeester, D.D. Klug, Ann. N. Y. Acad. Sci. 912 (2000) 859.
[34] T. Uchida, T. Hirano, T. Ebinuma, H. Narita, K. Gohara, S. Mae, R. Matsumoto, Environ. Energy Eng. 45 (1999) 2641.
[35] B. Chazallon, C. Focsa, J. Charlou, C. Bourry, J. Donval, Chem. Geol. 244 (2007) 175.
[36] E. Dartois, D. Deboffle, Astron. Astrophys. 490 (2008) 19.
[37] H. Ohno, M. Kida, T. Sakurai, Y. Iizuka, T. Hondoh, H. Narita, J. Nagao, Chem. Phys. Chem. 11 (2010) 3070.
[38] H.W. Schrotter, H.W. Klockner, Raman Spectroscopy of Gases and Liquids, Springer-Verlag, Berlin, 1999.
[39] P.S.R. Prasad, K.S. Prasad, N.K. Thakur, Curr. Sci. 90 (2006) 1544.
[40] J. Kortus, G. Irmer, J. Monecke, M.R. Pederson, Model. Simul. Mater. Sci. Eng. 8 (2000) 403.
[41] J.C. Seitz, J.D. Pasteris, B. Wopenka, Geochim. Cosmochim. Acta 51 (1987) 1651.
[42] K.C. Hester, R.M. Dunk, S.N. White, P.G. Brewer, E.T. Peltzer, E.D. Sloan, Geochim. Cosmochim. Acta 71 (2007) 2947.
[43] M.J. Frisch, G.W. Trucks, H.B. Schlegel, G.E. Scuseria, M.A. Robb, J.R. Chesseman, V.G. Zarzewki, J.A. Montgomery, R.E. Stratmann, J.C. Burant, S. Dapprich, J.M. Millam, A.D. Daniels, K.N. Kudin, M.C. Strain, O. Farkas, J. Tomasi, V. Barone, M. Cossi, R. Cammi, B. Mennucci, C. Pomelli, C. Adamo, S. Clifford, J. Ochterski, G.A. Petersson, P.Y. Ayala, Q. Cui, K. Morokuma, D.K. Malick, A.D. Rabuck, K. Raghavachari, J.B. Foresman, J. Cioslowski, J.V. Ortiz, B.B. Stefanov, G. Liu, A. Liashenko, P. Piskorz, I. Komaromi, R. Gomperts, R.L. Martin, D.J. Fox, T.A. Keith, M.A. Al-Laham, C.Y. Peng, A. Nanayakkara, C. Gonzalez, M. Challacombe, P.M.W. Gill, B.G. Johnson, W. Chen, M.W. Wong, J.L. Andres, M. Head-Gordon, E.S. Replogle, J.A. Pople, Gaussian 03 (RevisionA.1), Gaussian, Inc., Pittsburgh, PA, 2004.
[44] S.J. Clark, M.D. Segall, C.J. Pickard, P.J. Hasnip, M.J. Probert, K. Refson, M.C. Payne, Z. Kristallogr. 220 (2005) 567.
[45] J.M. Soler, E. Artacho, J.D. Gale, A. García, J. Junquera, P. Ordejón, D. Sánchez-Portal, J. Phys.: Condens. Mater. 14 (2002) 2745.
[46] B. Hammer, L.B. Hansen, J.K. Norskov, Phys. Rev. B 59 (1999) 7413.
[47] D.M. Ceperley, B.J. Alder, Phys. Rev. Lett. 45 (1980) 566.
[48] J.P. Perdew, A. Zunger, Phys. Rev. B 23 (1981) 5048.
[49] N. Troullier, J.L. Martins, Phys. Rev. B 43 (1991) 1993.
[50] M.V. Fernández-Serra, E. Artacho, J. Chem. Phys. 121 (2004) 11136.
[51] A. Hernández-Laguna, E. Escamilla-Roa, V. Timón, M.T. Dove, C.I. Sainz-Díaz, Phys. Chem. Miner. 33 (2006) 655.
[52] C.I. Sainz-Díaz, E. Escamilla, A. Hernández-Laguna, Am. Mineral. 90 (2005) 1827.
[53] J.S. Tse, J. Supramol. Chem. 2 (2002) 429.
[54] B. Delley, J. Chem. Phys. 113 (2000) 7756.
[55] Accelrys Software, Inc., Materials Studio, version 5.0, San Diego, CA, 2009.
[56] T.A. Halgren, W.N. Lipscomb, Chem. Phys. Lett. 49 (1977) 225.
[57] H. Heinz, R.A. Vaia, L. Farmer, J. Chem. Phys. 124 (2006) 224713.
[58] C.I. Sainz-Díaz, M. Francisco-Márquez, A. Vivier-Bunge, Theor. Chem. Acc. 125 (2010) 83.
[59] B.H. Besler, K.M. Merz Jr., P.A. Kollman, J. Comput. Chem. 11 (1990) 431.
[60] A.K. Rappé, W.A. Goddard, J. Phys. Chem. 95 (1991) 3358.
[61] A. Klapproth, Strukturuntersuchungen an Methan- und Kohlenstoffdioxid-Clathrat-Hydraten, Ph.D. Thesis, Georg-August-Universitat, Gottingen, Germany, 2002.
[62] H.J.C. Berendsen, J.P.M. Postma, W.F. Van Gusteren, A. DiNola, J.R. Haak, J. Chem. Phys. 37 (1984) 185.
[63] O. Teleman, B. Jonsson, S. Engstrom, Mol. Phys. 60 (1987) 193.
[64] A.K. Soper, Chem. Phys. 258 (2000) 121.
[65] R.W. Henning, A.J. Schultz, V. Thieu, Y. Halpern, J. Phys. Chem. A 104 (2000) 5066.
[66] S. Circone, L. Stern, S.H. Hirby, W.B. Durham, B.C. Chakoumakos, C.J. Rawn, A.J. Rondinone, Y. Ishii, J. Phys. Chem. B 107 (2003) 5529.
[67] C.A. Koh, R.E. Wesracott, W. Zhang, K. Hirachand, J.L. Creek, A.K. Soper, Fluid Phase Equilib. 194 (2002) 143.
[68] M.T. Kirchner, R. Boese, W.E. Billups, L.R. Norman, J. Am. Chem. Soc. 126 (2004) 9407.
[69] P. Kumar, N. Sathyamurthy, J. Phys. Chem. A 115 (2011) 14276.
[70] S. Grimme, J. Antony, T. Schwab, C. Muck-Lichtenfeld, Org. Biomol. Chem. 5 (2007) 741.
[71] W. Cantrell, G.E. Ewing, J. Phys. Chem. B 105 (2001) 5434.
[72] S. Subramanian, E.D. Sloan Jr., Fluid Phase Equilib. 158–160 (1999) 813.
[73] I.L. Moudrakovski, A.A. Sanchez, C.I. Ratcliffe, J.A. Ripmeester, J. Phys. Chem. B 105 (2001) 12338.
[74] H.C. Andersen, J. Chem. Phys. 72 (1980) 9173.
[75] C. Geng, H. Wen, H. Zhou, J. Phys. Chem. 113 (2009) 5463.
[76] Peters, et al., J. Am. Chem. Soc. 130 (2008) 17342.
[77] M. Rodger, Ann. N. Y. Acad. Sci. 912 (1990) 474.
[78] A. Gupta, S.F. Dec, A.K. Koh, E.D. Sloan Jr., J. Phys. Chem. C 111 (2007) 2341.
[79] D.R. Lide (Ed.), CRC Handbook of Chemistry and Physics. A Ready-reference Book of Chemical and Physical Data, 71st ed., CRC Press, Boca Raton, FL, 1990.
[80] C. Iuga, C.I. Sainz-Díaz, A. Vivier-Bunge, J. Phys. Chem. C 116 (2012) 2904.
[81] G.C. Pimentel, S.W. Charles, Pure Appl. Chem. 7 (1963) 111.
[82] B. Beeskow-Strauch, J.M. Schicks, Energies 5 (2012) 420.
[83] Y. Zhao, D.G. Truhlar, J. Chem. Theory Comput. 3 (2007) 289.
[84] N. Marom, A. Tkatchenko, M. Rossi, V.V. Gobre, O. Hod, M. Scheffler, L. Kronik, J. Chem. Theory Comput. 7 (2011) 3944.